Combined Frequency Control from Trains Thermal Inertia: An Assessment of Frequency Controllers Interaction

Jesús Araúz, Friedrich Wiegel, Simon Waczowicz, Veit Hagenmeyer, *Member, IEEE*, Sergio Martinez, *SeniorMember, IEEE*

***Abstract*—The increasing introduction of power electronics into electric power systems requires more effort to maintain the stability, reliability, and security of grids. Among these, the frequency stability is worsened by the displacement of conventional generators. Demand response has been considered as an alternative to ensure grid stability. The present work proposes a combined frequency control for railway systems to support grid ancillary services without risking the circulation of trains and the comfort of passengers. In contrast to current demand response algorithms, it provides primary and secondary frequency control, and virtual inertia. In addition, due to the rising dynamics complexity in grids, this work presents a performance-based methodology to assess the interaction among frequency controllers without needing detailed models. Simulation and experimental case studies are presented to exemplify and validate the proposed method. The results demonstrate the effectiveness of the methodology in allowing a fast and low-complexity assessment. In addition, the benefits of the proposed control are demonstrated by several performance metrics. The coherence between simulation and experimental results validates the reliability and implementability of the proposed method in a real microgrid.**

***Index Terms*—Frequency control, Thermal inertia, Railway, Demand response, Hardware-in-the-Loop.**

I. Introduction

THE interest in using renewable energy resources for electrical power generation has increased in recent decades. The successful integration of renewable energy sources into electrical grids involves overcoming a variety of challenges, including political, technical, and social obstacles [1].

This research was funded in part by the Panamanian Secretaría Nacional de Ciencia, Tecnología e Innovación (SENACYT), grant number 270-2022-108, in part by the Spanish national research agency Agencia Estatal de Investigación, grant number PID2019-108966RB-I00/AEI/10.13039/501100011033, and in part by the Helmholtz Association under the Program Energy System Design.

Jesús Araúz is with the Escuela Técnica Superior de Ingenieros Industriales (ETSII), Universidad Politécnica de Madrid (UPM), C/José Gutiérrez Abascal, 2, 28006, Madrid, Spain; the Panama Railway Engineering Research Group, Faculty of Electrical Engineering, Universidad Tecnológica de Panamá (UTP), Panama City, 0819-07289, Republic of Panama; and the Research group Energy and Comfort in Bioclimatic Buildings, Faculty of Mechanical Engineering, UTP, Panama City, 0819-07289, Republic of Panama (e-mail: jesus.arauz@alumnos.upm.es).

Friedrich Wiegel (e-mail: friedrich.wiegel@kit.edu), Simon Waczowicz (e-mail: simon.waczowicz@kit.edu), and Veit Hagenmeyer (e-mail: veit.hagenmeyer@kit.edu) are affiliated with the Institute for Automation and Applied Informatics (IAI), Karlsruhe Institute of Technology (KIT), 76131, Karlsruhe, Germany.

Sergio Martinez is with the ETSII, UPM, C/José Gutiérrez Abascal, 2, 28006, Madrid, Spain (e-mail: sergio.martinez@upm.es).

Manuscript received xxxx xx, 202x; revised xxxx xx, 202x.

A. The Big Picture

In terms of technical challenges, grids with high penetration of intermittent resources and power electronics converters present different characteristics from traditional ones. The converter controls mostly determine the dynamics under faults, during transients, and in the steady state. These dynamics are characterized by multiple and diverse time constants. The power of the primary power source is practically decoupled from the electromagnetic power of the grid, thus leading to a null inertial response. In general, electric generators connected to the grid through power electronic converters present a dynamic behavior different from conventional generators. As expected, these distinctions influence stability problems [2].

Angle stability is affected by the change in power flows, the displacement of large synchronous generators, and the location of the new converter-interfaced generation. Voltage stability can be affected in the short and long terms due to converters' fast-acting and power limits. Frequency stability is mainly affected by the decrease in inertia. Converter-interfaced generation does not intrinsically provide inertia and primary frequency control. Furthermore, some economic aspects of renewable-based generation restrict the possibility of power curtailment. Thus, frequency control in low-inertia grids faces new difficulties, driven by the extent of the frequency deviations, the increase in the rate of change of frequency (ROCOF), and the reduction of inertia, leading to a more oscillatory behavior in the grid [3]. However, it has been widely demonstrated that, with adequate controllers, converters can provide frequency control [4].

B. Related work

Extensive research has been conducted on frequency control strategies. For example, a good review can be found in [3], where the strategies are classified into three categories: generation-based, transmission-based, and load-based. The first category includes classical trends for conventional generators and current trends for photovoltaics (PV) and wind generators. Most studies have focused on deloading, power curtailment, DC-link capacitors, delta power, and inertia emulation. The second category includes the use of inducverters and virtual synchronous generators (VSG), energy storage systems (pumped hydro, supercapacitor, flywheel, battery, and compressed air, among others), and dynamic thermal rating. The last category includes load modulation, energy storage

systems, and under-frequency load shedding (UFLS). However, in the literature, it is evident that there are few studies on frequency control demand response approaches.

Several authors have studied how loads can operate smartly to provide virtual inertia [5]–[7]. The authors of [5] highlighted the feasible contribution of inertia from DC links and energy storage systems. In [6] and [7], the authors proposed loads that can actively change their consumption depending on the voltage values to mitigate fluctuations in the AC and/or DC grids. Electric vehicles have also been considered for providing frequency control. The authors of [8] used the power hardware-in-the-loop (PHIL) technique to demonstrate how to reduce frequency deviations in a microgrid employing decentralized coordinated control of the state of charge and the scheduling. In [9], the authors proposed a robust mixed controller for making electric vehicles contribute effectively to load frequency control under different scenarios and high uncertainty, thus partially relieving conventional generation from this task. The authors of [10] proposed a new design for providing frequency and voltage control to the public grid from electric vehicles. The proposed method presents low computational cost and low-complexity modeling and is experimentally validated using the PHIL technique.

Recently, railway systems have been considered potentially relevant grid elements that can provide benefits to the public grid. Apart from many studies focusing on the railway electrification system as an energy hub (distributed and renewable generation, energy storage systems, and connections to the grid, among others) [11], railways can also be considered as adjustable loads. In [12] authors proposed the use of the thermal inertia of trains to provide primary frequency control through heating, ventilation, and air conditioning (HVAC) systems onboard trains. The authors of [13] also proposed the use of HVAC systems including the provision of virtual inertia. In [14] authors oriented the foundations established in [12] to relieve renewable generation from frequency control tasks. The authors of [15] studied possible combinations of primary and supplementary frequency controls using a low-computational-cost tuning methodology. Previous studies investigated the use of onboard HVAC systems to provide different frequency controls. However, as noted in the literature review, most studies on frequency control-based demand response approaches do not consider providing combinations of more than two frequency controls. Thus, no insights into the interactions between the control schemes and tuning have been provided.

The present work intends to fill this gap when more than two frequency control strategies from loads are combined and the study of the interactions among demand response frequency controllers is needed. For this, on the one hand, a new frequency control scheme for allowing railway systems to support grid frequency is introduced. It comprises a combination of primary and supplementary frequency controls with virtual inertia. On the other hand, a frequency performance-based assessment methodology is proposed. This allows the study of the impact of each frequency control scheme on the grid frequency behavior. Although both the frequency control scheme and methodology are introduced in a railway-based framework, it is worth mentioning that they can be applied to different types of consumptions and control algorithms.

In addition, the PHIL technique was used to test the implementation of frequency controls. Real noise, delays, and non-linear characteristics must be addressed by the proposal. Its performance in a real environment is built up with real electrical machines, loads, converters, controls, and connections. Additionally, it corroborates the coherence of the results provided by the computational application of the proposed methodology.

The remainder of this paper is structured as follows. Section II describes the scope, composition, and purpose of the methodology. It includes methods for modeling power systems (Section II-A); railways, including the proposed frequency control scheme, (Section II-B); and controller interaction studies (Section II-C). Section III presents a case study using real training data. This includes a computational simulation (Section III-A) and an experiment in a real microgrid (Section III-B). Finally, Section IV summarizes the contributions, findings, challenges, and future work.

II. METHOD

A controller interaction assessment requires the description of system dynamics, power systems, and railways, and an exhaustive analysis of their couplings. This requires a high computational effort and sufficient background on the operation of both systems. However, an intermediate complexity level, focused on the performance of the variables of interest, can be suitable for achieving realistic behaviors.

Toward this goal, in this paper, we propose a methodology that includes: the modeling of systems (i.e., controllers, devices, etc.); the selection of objective functions, relevant parameters, and operation ranges; and the use of mathematical and/or statistical procedures to assess the performance of objective functions. A more detailed model may be appropriate depending on the scope of the study.

A. Power system modeling

As seen in the literature review of Section I-B, many studies have focused on frequency control using low-frequency control schemes to simplify modeling and accelerate the analysis of frequency behavior. A model based on Kirchhoff's laws is proposed for implementation in real grids [16]. This allows for the interaction of voltages and currents as well as the effect of more detailed dynamics.

The foundation for modeling the most common power system elements (e.g., lines, transformers, FACTS, electrical drives, and loads) is well described in [16]. Some previous studies, such as [11], also require the modeling of distribution lines due to their scope. Although almost every power system component may influence the frequency performance, it is proposed to focus on standard synchronous generators (SGs) because they mainly define the frequency behavior.

One of the models presented in [17] for stability analysis is considered. This model comprises the dynamics of stator, rotor, and damper windings. Mechanical power and field voltage are required as inputs. The voltage vector in the rotor reference frame can be obtained from (1), in per unit, where

s is the Laplace operator. $[V_{SG}]$ vector includes the stator, field, and damper winding voltages along dq axis. $[R]$ is a diagonal matrix of the resistance of the windings in dq axis. $[i]$ is the current vector. $[L]$ is the matrix of the self and mutual inductances in dq axis. $[W]$ is the rotor speed matrix, where all the elements are zero except $W(1,2) = w_r$ and $W(2,1) = -w_r$. It is worth mentioning that depending on the rotor type (salient-pole or round), the size of matrices can change. Equation (2) shows the rotor speed (w_r) calculation in per unit, where H is the SG inertia coefficient in seconds. T_m denotes the mechanical torque generated by the prime mover. T_e is the electromagnetic torque. F_r represents the friction coefficients.

$$[V_{SG}(s)] = [R][i(s)] + s\left([L][i(s)]\right) + [W(s)]([L][i(s)]) \quad (1)$$

$$\begin{aligned} w_r(s) &= 1 + \frac{T_m(s) - T_e(s) - F_r\, w_r(s)}{2Hs} \\ &= \frac{2Hs + T_m(s) - T_e(s)}{2Hs + F_r} \end{aligned} \quad (2)$$

The mechanical torque variations, ΔP_m, can be modeled based on the prime mover dynamics. Equation (3), in per unit, groups several simplified models of the most common prime movers used in [16], [18]. The variation in the gate (valve or injector) opening is denoted by ΔOp. There, τ is the time constant, and F is the power fraction. The subscripts wa, hp, rh, ch, v, f, cd, and c refer to the water flow path in the hydraulic turbines; high-pressure, re-heater, and main inlet volume in steam turbines; valve, fuel supply, and compressor discharge in gas turbines; and combustion in diesel engines; respectively. The governing system of each generation technology can also be found in [16], [18], [19].

$$\frac{\Delta P_m}{\Delta Op} = \begin{cases} \frac{1-\tau_{wa}s}{1+0.5\tau_{wa}s} & \text{, hydro turbine} \\ \frac{1+F_{hp}\tau_{rh}s}{(1+\tau_{ch}s)(1+\tau_{rh}s)} & \text{, steam turbine} \\ \frac{1}{(1+\tau_v s)(1+\tau_f s)(1+\tau_{cd}s)} & \text{, gas turbine} \\ e^{-\tau_c s} & \text{, diesel engine} \end{cases} \quad (3)$$

To achieve stabilized SG operation, an excitation system and a power system stabilizer (PSS) are also required. Depending on the SG topology, there are several excitation system possibilities [20]. PSS topologies are also presented in [20]. However, a generic PSS model (4), in per unit, may be suitable for most frequency control studies. V_{PSS} is the output signal of the PSS, which is added to the voltage reference of the excitation system. The first quotient includes the rotor speed deviation (Δw_r), overall gain (k_{PSS}), low-pass (lp) filter, and high-pass (hp) filter. The second quotient includes two lead-lag filters. The time constants of the first filter, τ_{a1} and τ_{a2}, are much smaller than the ones of the second filter, τ_{b1} and τ_{b2}.

$$V_{PSS}(s) = \frac{\Delta w_r(s) k_{PSS}\, \tau_{hp} s}{(1+\tau_{lp}s)(1+\tau_{hp}s)} \frac{(1+\tau_{a1}s)(1+\tau_{b1}s)}{(1+\tau_{a2}s)(1+\tau_{b2}s)} \quad (4)$$

B. Railway system modeling

The authors of [21] broadly describe the topology of the most relevant railway systems worldwide. Based on the desired railway system for modeling, many considerations must be taken into account. Because of the scope of the present work and previous railway studies on frequency control, a DC railway system model is preferred. It is worth mentioning that, in addition to the railway and frequency control topology under study, the electrical coupling with the power system is approximately the same if an AC railway is modeled (except for the rectifiers, that are not needed).

1) Electrical modeling: DC railway system electrical models have been extensively implemented over time [22]. Recently, they were tested using the PHIL technique, thus validating many proposed models [23]. Electrical modeling can be divided into two parts: electrification system and trains. On the one hand, the first is mainly composed of the connection to the grid, a step-down transformer (three- or single-phase, depending on topology), an uncontrolled rectifier (six or twelve pulses, commonly), and the catenary (including feeders, contact line, rails, etc.). For frequency control studies, it is feasible to neglect high-frequency phenomena that require more details on the conductors, semiconductors, and magnetic core models. Therefore, the traditional models of power electronics [24], conductors, and electrical machines can be used.

On the other hand, trains can be described in detail as required, as noted in the literature [11], [23], [25]. However, a lumped model (5), in SI units, is typically used to obtain the instantaneous power requirements. Here, $P_{e.train}$ is the electrical power of a single train. The first addend represents the consumption due to circulation. F_{res} is the total resistance force (bearing drag, friction, track deformation, aerodynamics, slopes, tunnels, and curvature [11]). $m\,a$ is the product of the mass and acceleration of the train. v is the train speed. η_{glo} is the power conversion efficiency, and γ is an auxiliary term used to differentiate the power flow from traction ($\gamma = 1$) to braking ($\gamma = -1$) operations. P_j is the j^{th} out of n auxiliary consumptions. Finally, P_{HVAC}, represents the electric power consumption of the HVAC systems.

$$P_{e.train} = \frac{(F_{res} + m\,a)\,v}{(\eta_{glo})^{\gamma}} + \sum_{j=1}^{n} P_j + P_{HVAC} \quad (5)$$

For multi-train operation modeling, the approaches in [23] and [25] can be applied. Each train power is calculated individually, as in (5), and is set as the setpoint of the current source. By means of power flow algorithms, the aggregation of all consumptions in the railway system as seen by the grid ($P_{railway}$) is obtained.

To provide grid frequency control, it is not necessary to simultaneously calculate the power system dynamics and electric consumption of trains due to motions. This is because the power of HVAC systems has been considered to provide frequency control [12]–[15], and the motions and any other consumption will not present relevant changes over time due to power system performance. Therefore, the approach proposed in [11] can be implemented. Thus, the power profile of the railway system can be calculated separately and coupled with the power system model in a single system experiment. Finally, by the quotient between the per-phase power ($P_{railway}/3$) and the phase to neutral RMS voltage at the public grid

node (V_{node}), a classical current injection model, $I(t) = (P_{railway}(t)/3)/V_{node}(t)$, can be applied, where $I(t)$ is the line RMS current (changing over time) at unity power factor.

2) Thermal modeling: The process of thermal modeling of trains is presented in [12]–[15]. This is based on a previous study of [26]. A one-dimensional second-order lumped model was used. There is one differential equation for each thermal system: the wagon inner air and the wagon mass. The air volume of each train is lumped into one air point, and the bogies and mechanical joints, among other components, into one body point. Equations (6) and (7), [12], [13], [15], in SI units, describe the dynamics of the air temperature (T_a) and train mass temperature (T_t), respectively. UA is the product of thermal transmittance and the related surface, where the interactions between different parts of the thermal model are represented by the following subscripts: ta (train mass – inner air), oa (outside air – inner air), and at (inner air – train mass). TM is the thermal mass, where the subscripts a and t represent inner air and train mass, respectively. T_o denotes the outside temperature. $\dot{Q}_k$ and $\dot{Q}_l$ represent the heat gains associated with the k^{th} and l^{th} components, respectively, within the systems that involve q and p heat gains. These heat gains contribute to changes in the temperature of the inner air and the train body. COP_{mean} is the average Coefficient Of Performance of the HVAC system, defined as the ratio between the thermal power delivered and the electric power consumed.

$$\frac{dT_a}{dt} = \frac{U_{ta}A_{ta}}{(TM)_a}(T_t - T_a) + \frac{U_{oa}A_{oa}}{(TM)_a}(T_o - T_a) + \frac{\sum_{k=1}^{q}\dot{Q}_k - (COP_{mean})P_{HVAC}}{(TM)_a} \tag{6}$$

$$\frac{dT_t}{dt} = \frac{U_{at}A_{at}}{(TM)_t}(T_a - T_t) + \frac{\sum_{l=1}^{p}\dot{Q}_l}{(TM)_t} \tag{7}$$

Equation (8), [12], [13], [15], in SI units, describes the mathematical approach used to relate the grid frequency deviations (Δf) to P_{HVAC}. As highlighted in [13], this approach considers a simplified model of an HVAC system. This means that the exact method of modifying the HVAC operation has not been studied. It has been found in the literature that by adjusting the operation of converters that control compressors, pumps, and valves, it is possible to allow thermal-fluidic systems to provide frequency control [27]–[30]. In (8), ρ is the air density, C_p is the specific heat at constant pressure, $\dot{V}$ is the injected air flow rate, and T_{set} corresponds to the setpoint temperature of the HVAC system.

$$P_{HVAC} = \frac{\rho\, C_p\, \dot{V}(T_{set}(\Delta f) - T_a)}{COP_{mean}} \tag{8}$$

As noted in Equation (8), T_{set} varies according to Δf. In contrast with previous works, for the first time, here we propose to provide primary and supplementary frequency control, and virtual inertia simultaneously from the load side, specifically from HVAC systems onboard trains. Equation (9), in SI units, describes the basis of the proposed control for making the electric consumption of HVAC systems responsive to the grid frequency state. The primary control is based on [12], the supplementary on [15], and the virtual inertia on [13]. Then, C_1, C_2, and C_3 are the gains for the three mentioned frequency controls, respectively. The function $g(T_a, \Delta f_{DB_2})$ is used to reset the integral term when T_a exceeds the comfort band or when Δf_{DB_2} changes from any value to zero. $g(T_a, \Delta f_{DB_2})$ is equal to the supplementary control when resetting, being zero otherwise. T_{rated} is the normal set-point temperature, i.e., the value of T_{set} if just the thermal comfort of passengers is considered (without using T_{set} as a manipulated variable for frequency control).

$$\begin{aligned} T_{set}(t) = &- C_1 \Delta f_{DB_1}(t) \\ &- C_2 \int \Delta f_{DB_2}(t)dt + C_2\, g(T_a, \Delta f_{DB_2}) \\ &- C_3\, d(\Delta f_{DB_3})/dt + T_{rated} \end{aligned} \tag{9}$$

As part of the proposal, each frequency control operates with different dead bands, contrary to what is usually implemented. The terms Δf_{DB_1}, Δf_{DB_2}, and Δf_{DB_3} are equal to Δf when it exceeds the corresponding dead bands ($DB_1, DB_2, or DB_3$) and zero otherwise. This way, each control can be properly tuned according to the frequency behavior imposed by the system. The results in [15] suggest the need for different dead bands. However, this aspect has not been explored yet.

C. Interaction among controllers

As stated in Section I, the present work proposes a method for analyzing the interactions among the frequency controllers of controllable loads. In the literature, most of demand response approaches implement their controls based on simplified mathematical equations that represent system behavior. However, modern power systems are being increasingly influenced by complex and unknown dynamics. Some of these may endanger the system operation and stability.

Some authors have developed new control algorithms and methods for determining their setups. In [18] authors proposed the use of a Student Psychology-Based Algorithm to optimally tune a diesel generator in a hybrid low-inertia grid. The authors of [31] analyzed the negative interaction between some FACTS control loops (current and PLL) and VSG, and proposed a solution. In [32] authors presented a method for the synchronization, active power regulation, and inertia provision of a VSG, improving the stability of the grid in a system with a low short-circuit ratio.

Among other works, managing all system information or using simplifications is required to assess the performances. Due to the possible lack of knowledge of system characteristics, non-deterministic methods are suggested for use. These are based on probabilistic and statistical methods. In recent years, sensitivity analysis-based approaches have been used for power flow and stability analysis [33]. Then, it is proposed to apply similar techniques to study the influence of the parameters of different frequency controllers of distinct devices on frequency performance metrics. Furthermore, this can be applied to study the mutual impact among control schemes of generators and controllable loads, such as onboard HVAC systems of trains.

A general workflow in sensitivity analysis starts with generating parameters samples (design of experiment principles, probability distributions, etc.), followed by defining the requirements to be fulfilled (i.e., creating cost functions), and, finally, evaluating the requirements with the values of the parameters (e.g. using Monte Carlo simulations). Subsequently, the results can be statistically analyzed to determine correlations and define the relevance of the parameters [34]. For example, (10) is a widely used measure for sensitivity analysis. It is a standard deviation (σ)-based normalized form, where $S^{\sigma}_{z_u}$ is the sensitivity of the u^{th} factor of the Z factor array, and Y is the output vector.

$$S^{\sigma}_{z_u} = \frac{\sigma_{z_u} \partial Y}{\sigma_Y \partial z_u} \tag{10}$$

III. Case Study

The case study system is composed of two main parts: a railway system model and a power system. The first part, railway, is adapted from previous works [12]–[15]. It is a model inspired by the characteristics of the Panama Metro Line 1 (PML1). The model is extensively detailed in [11]. The adapted version consists of two tracks, four trains, three traction substations, and five passenger stations. To evaluate the frequency control in low-inertia grids, the power system is formed by one SG and a resistive load, in addition to the railway feeder. The thermal comfort band to limit the HVAC system operation is $T_{rated} \pm 2.5\,^{\circ}\mathrm{C}$, as set in previous works ($T_{rated} = 26\,^{\circ}\mathrm{C}$) [12]–[15].

The case study also compares the effect of the intrinsic uncertainty of reality (i.e., uncertainties due to commercial components' imperfections, unrepeatable conditions, etc.) with that of computational simulations. The computational simulation allows the study of multiple scenarios and determines the relations among the control parameters and selected metrics. The experimental test proves the effectiveness of the proposed control, supports simulation results, assesses the frequency performance of real systems under the proposed demand response contribution, and estimates the behavior of the HVAC systems during their contribution, among other aspects.

To compare the results obtained by simulation and experimentation, a gray-box approach is considered (i.e., to neglect detailed specs by aiming at main patterns). Equation (11), in per unit, is an elaboration of (2) to show the frequency deviation evolution taking into account the interaction among load deviations ($\Delta P_L(s)$), equivalent inertia of rotating machines ($H_{eq}(s)$), inherent equivalent grid damping factor (D_{eq}), lumped effect of dynamics and control schemes of generators ($G(s)$), and controllable loads ($L_c(s)$) sensitive to frequency deviations.

$$\Delta f(s) = -\frac{\Delta P_L(s)}{2H_{eq}s + D_{eq} + L_c(s) - G(s)} \tag{11}$$

The exact $G(s)$ and H_{eq} may not be obtained in real grids and commercial equipment, as it is confidential information. Furthermore, an accurate value for D_{eq} cannot be obtained at all, as it is an overall description of the frequency dependency of all the loads of a power system. Therefore,

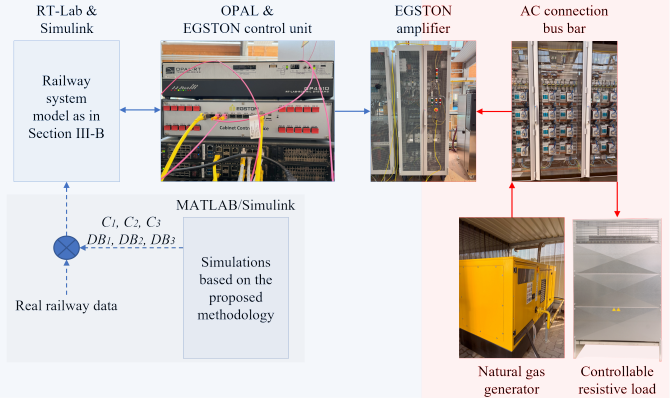

Fig. 1: Interaction between simulation and experimental tests: power (red), data (blue), real-time flow (solid arrows), data transmittable online and offline (dashed arrows).

the simulation and experimental frequency behaviors can not be exactly the same. However, a similar response under the proposed frequency control can be achieved. Since the proposed methodology for analyzing interactions claims that many of them can be assessed only using performance metrics, a highly detailed computational model may not be critical. The computational model should match the overall frequency response for a specific load event. Specifications from real machines are included, and the railway model, along with the HVAC system and the frequency control proposal, is also the same in simulation (Section III-A) and experimental (Section III-B) tests. In both tests, a sudden load shedding of 10 kW produces a maximum frequency deviation around 1.2 Hz. Similar interactions are observed in both tests.

The gas-based generator (GG) and the resistive load presented in [35] are used. The GG is a 56 kVA, 4-pole, salient-pole, and self-excited synchronous machine driven by a 56.8 kW natural gas generator. This set presents a constant power fluctuation which poses a random frequency deviation around ± 0.3 Hz. Fig. 1 shows the overall case study scheme. Although simulation and experimental tests are not carried out simultaneously, the results of the first one are expected to provide similar performance in the environment of the latter.

Many metrics can be used to assess the frequency performance [18]. For this study, the average absolute frequency deviation ($|\Delta f|_{ave}$), the accumulative absolute frequency deviation ($|\Delta f|_{accu}$), the average absolute ROCOF ($|ROCOF|_{ave}$), and the maximum absolute frequency deviation ($|\Delta f|_{max}$) are used.

A. Computational simulations

The simulation is carried out in Simulink®. It is used to build the power and railway system models, both based on Section II equations and the implementation presented in [12]. The sensitivity analysis is performed using the *Simulink Design Optimization Toolbox* and the *Statistics and Machine Learning Toolbox*.

By studying the dynamics of the simplified HVAC system model, it is possible to determine the relation between power

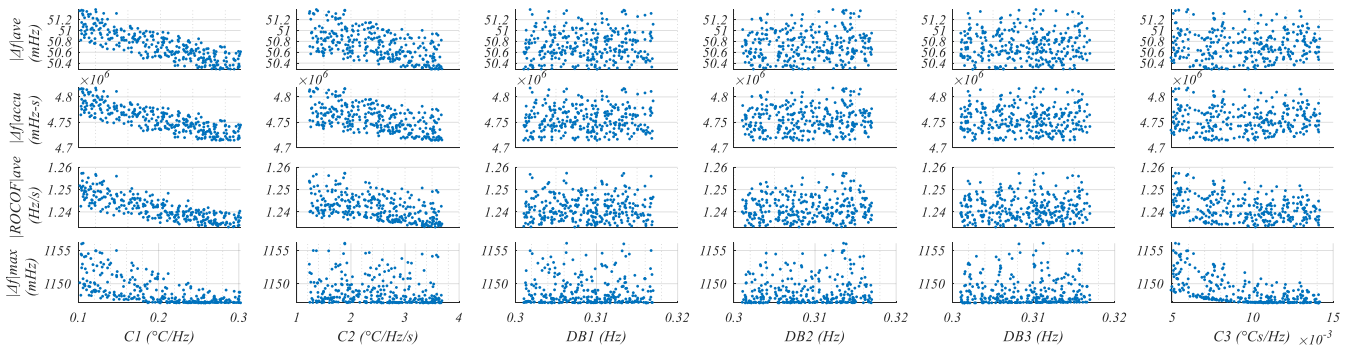

Fig. 2: Sensitivity analysis results: variation of selected metrics due to the control parameters value.

and set-point temperature. Each coefficient C_1, C_2, and C_3 is obtained by considering the maximum frequency deviation, ROCOF, and accumulative frequency deviation, with similar iterative procedures to those in [13], [15]. Subsequently, a range between 50% and 150% for each one is established. Finally, their ranges are: 0.0943 °C/Hz $\leq C_1 \leq$ 0.2828 °C/Hz, 1.1475 °C/Hz/s $\leq C_2 \leq$ 3.4426 °C/Hz/s, and 0.0047 °Cs/Hz $\leq C_3 \leq$ 0.01422 °Cs/Hz. The range of dead bands (DB_1, DB_2, and DB_3) is set considering the ones in [36], the results in [13], [15], and the generator technical restrictions. This is, from ± 0.301 Hz to ± 0.317 Hz. The dataset includes 300 combinations of the six control parameters. This is obtained by applying a uniform distribution to the selected ranges. The base case is defined as the median of each parameter range.

Fig. 2 shows the results of the selected metrics for each combination. At first glance, some parameters, such as C_1 and C_2, have a greater influence on the performance metrics. C_3 also presents a monotonic relationship with some metrics in specific parts of its range. Dead bands do not present a coherent and constant relation to the metrics. They seem to provide similar results with very different values. As well known in the literature, standalone C_1 and C_2 should present a strong linear behavior in all metrics. In addition, C_3 is expected to present a clear non-linear behavior, mainly in $|ROCOF|_{ave}$. These initial results demonstrate the mutual influence among the controllers, where their normal behaviors are not presented. The mutual influence among controllers alters their individual impacts on system performance. The effect of dead bands and the combination of different values cause the responses to be more scattered than expected. Dead bands introduce non-linear and context-dependent effects on the metrics. As mentioned in [15], [36], the relation between frequency control gains and the dead band is not linear and is highly influenced by the operation ranges. Interactions between controllers lead to more scattered responses than standalone analyses would suggest. Evidently, the presence of other controllers modifies the impact of others on the metrics. In summary, the combined effects of control parameters must be considered for accurate system tuning.

Total and partial correlations can be calculated to assess the influence of control parameters on the frequency performance metrics. For this, the Pearson and Spearman correlation coefficients are used. Equation (12) shows the calculation of the Pearson Coefficient (C^{pe}). For this, the operator cov is the covariance. X can be any of the studied parameters and M_f can be any of the chosen metrics to assess the grid frequency performance. Pearson correlation is used for linear behaviors. For monotonic behavior, the Spearman coefficient (C^{sp}) is preferred [37]. It uses the same equation but requires Rank transformation to variables $(R(X), R(M_f))$.

$$C^{pe} = \frac{cov(X, M_f)}{\sigma_X \sigma_{M_f}} \tag{12}$$

Analyzing the correlations between the control parameters and performance metrics allows to assess the impact of these parameters on frequency performance and the interactions among them. Table I shows the total correlation coefficients, C^{pe} and C^{sp}, and the partial coefficients, $C^{pe}_{partial}$ and $C^{sp}_{partial}$. Because of the nature of the load event and control topology, $|\Delta f|_{ave}$ and $|\Delta f|_{accu}$ share the same sensitivity results. Partial correlations describe the impact of a parameter over a specific metric, without considering the impact of the other parameters [34]. The appropriate selection of metrics and ranges can simplify the interaction study. Because the *Pearson* and *Spearman* coefficients are quite similar, all behaviors are monotonic and linear in the selected ranges. This comparison shows a reduction in the complexity of the analysis. C_1 and C_2 present the largest partial correlations for every metric. However, C_2 does not influence much $|\Delta f|_{max}$. C_3 influences $|\Delta f|_{max}$, more than C_2, and $|ROCOF|_{ave}$. DB_3 is the only dead band with non-negligible impact, as seen in $|ROCOF|_{ave}$. However, the correlation is not strong, as shown in Fig. 2. The differences among total and partial coefficients demonstrate how one controller is affected by the others. All partial coefficients in the most relevant parameters, according to the criteria used, are smaller than the total coefficients. C_1 impact is decreased by 15% in $|\Delta f|_{ave}$, $|\Delta f|_{accu}$, and $|ROCOF|_{ave}$, and by 25% in $|\Delta f|_{max}$. C_2 impact is decreased by 39% in $|\Delta f|_{ave}$ and $|\Delta f|_{accu}$, by 45% in $|ROCOF|_{ave}$, and by 31% in $|\Delta f|_{max}$. C_3 impact is decreased by 63% and 25% for $|ROCOF|_{ave}$ and $|\Delta f|_{max}$, respectively. Then, it is clear that C_1 dominates the combined frequency control effect on the metrics, except for $|\Delta f|_{max}$. In this case, C_3 has almost the same theoretical impact.

To appreciate the benefits of the proposed control, intuitive configurations are extracted and studied individually, as shown

TABLE I: SENSITIVITY ANALYSIS RESULTS: PERCENTAGE CORRELATION.

Control parameters	$\|\Delta f\|_{ave}$	$\|\Delta f\|_{accu}$	$\|ROCOF\|_{ave}$	$\|\Delta f\|_{max}$
	$C^{pe}, C^{pe}_{partial}, C^{sp}, C^{sp}_{partial}$			
C_1	-81.57, -96.55, -81.81, -96.12	-81.57, -96.55, -81.81, -96.12	-80.43, -95.93, -81.47, -96.98	-63.54, -82.34, -68.16, -90.96
C_2	-56.55, -92.82, -56.00, -91.78	-56.55, -92.82, -56.00, -91.78	-48.22, -88.20, -50.85, -91.66	-16.51, -24.05, -23.55, -49.24
C_3	0.53, 6.84, 3.56, 16.53	0.53, 6.84, 3.56, 16.53	-30.52, -78.93, -28.97, -79.05	-60.94, -81.24, -61.61, -89.31
DB_1	4.54, 6.18, 4.26, 1.88	4.54, 6.18, 4.26, 1.88	1.59, 3.68, 2.11, 1.86	-1.83, 3.67, -2.56, -0.54
DB_2	8.22, 12.42, 7.49, 8.91	8.22, 12.42, 7.49, 8.91	6.52, 4.48, 5.44, -0.11	8.18, 9.00, 7.31, 9.00
DB_3	0.63, 9.33, -0.11, 5.69	0.63, 9.33, -0.11, 5.69	4.18, 24.98, 3.53, 25.45	-0.25, 4.08, 2.48, 14.54

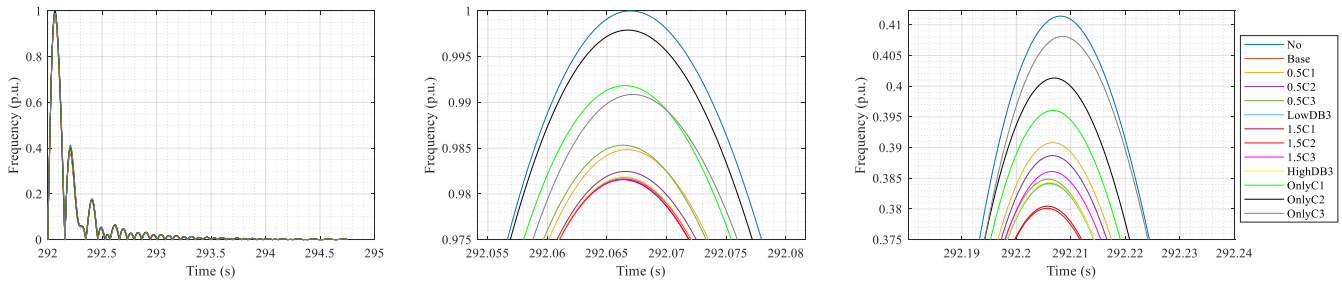

Fig. 3: Absolute frequency deviation evolution under different control setups referred to the maximum value. Left plot shows the general evolution. Middle plot shows a detail of the first oscillation. Rigth plot shows a detail of the second oscillation.

in Fig. 3. Cases $0.5C_{1,2,3}$ and $1.5C_{1,2,3}$ represent a decrement or increment of 50%, respectively, to the specific gain in the base case. The low and high DB_3 cases are the base cases, but the lowest or highest values of the DB_3 range are selected, respectively. Only $C_{1,2,3}$ cases represent standalone controllers. The *per unit* absolute frequency deviation of the system following a sudden load shedding is shown. It is evident that all considered configurations improve the frequency behavior compared to the case with no frequency control (blue line). In general, the base setup plus 50% performs the best. Followed by a base setup minus 50% and by the standalone controllers. This result is consistent with the findings of previous works [12]–[15].

B. Experimental validation

The tests are carried out in the Energy Lab [35]. As shown in Fig. 1, the grid-forming GG, resistive load, and amplifier interact using an AC busbar. The amplifier is a DC/AC converter that operates as the current source and amplifies the current setpoints provided by the HIL device. This behavior is based on the model loaded through RT-Lab®, which is the same railway model used in Section III-A.

Fig. 4 shows the computation of the selected metrics for the event described in Section III. The control setups in Fig. 3 were applied. The vertical axis represents the percentage variation of a metric compared with the base case results. Positive variations mean increments. Exceeding the corresponding dashed lines means worsen the metric compared to the case with no frequency control. In next results, cases with asterisk (*) should be compared only with their corresponding dashed line to determine their trend. Not all the cases improve the frequency performance. Those with reduced gains and standalone controllers slightly worsen the performance. However, most cases represent larger improvements than simulation results, particularly with a high presence of C_3, the virtual inertia control in (9). As in the simulation, $|\Delta f|_{ave}$ and $|\Delta f|_{accu}$

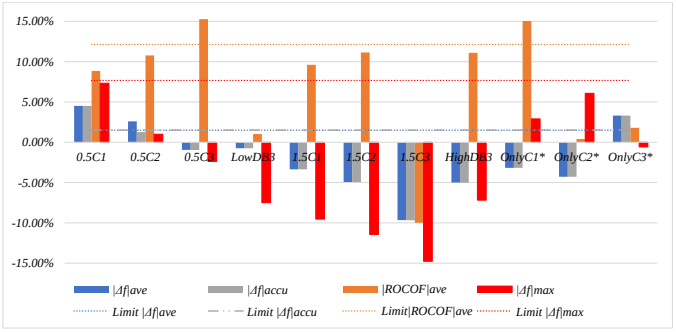

Fig. 4: Experimental results: percentage metrics variation in control setups compared to base case (section III) results. The dashed lines represent the limit of performance improvement.

share a very similar performance across tests. $|\Delta f|_{max}$ varies similarly but more aggressively because of the higher relevance of C_3, as noted in Table I. However, $|ROCOF|_{ave}$ presents a more scatter behavior in its performance. Here, the unpredictable effects of dealing with a real GG are appreciated. As stated in Section III, the degree of oscillation and noise affects the virtual inertia controller (derivative term in (9)).

Fig. 5 shows the results for a better assessment of the experimental tests. It shows the same results as Fig. 4, but includes a comparison with the metrics obtained in the simulation (Fig. 3). As previously mentioned, the tested systems were not the same. Thus, the magnitudes of the metrics are not expected to be similar, only the trend should be. The horizontal lines are the corresponding limits of performance improvement defined by the cases without frequency control in the experimental and simulation tests. The $0.5C_{1,2,3}$ cases tend to worsen the frequency performance, whereas the $1.5C_{1,2,3}$ tend to improve it. Most of the experimental and simulation variations match their trends. However, the effect of noise inverted the expected impact of C_3, mainly in $|ROCOF|_{ave}$ results. As

TABLE II: SIUMULATION VS. EXPERIMENTAL RESULT TRENDS.

Tests description	$\|\Delta f\|_{ave}$	$\|\Delta f\|_{accu}$	$\|ROCOF\|_{ave}$	$\|\Delta f\|_{max}$
	Simulation (correlation) vs. Experimental			
$0.5C_1$	increase (high) vs. increase	increase (high) vs. increase	increase (high) vs. increase	increase (high) vs. increase
$0.5C_2$	increase (high) vs. increase	increase (high) vs. increase	increase (high) vs. increase	increase (low) vs. increase
$0.5C_3$	increase+ (low) vs. decrease	increase+ (low) vs. decrease	increase (high) vs. increase	increase (high) vs. decrease
Low DB_3	decrease (low) vs. decrease	decrease (low) vs. decrease	decrease (low) vs. increase	decrease (low) vs. decrease
$1.5C_1$	decrease (high) vs. decrease	decrease (high) vs. decrease	decrease (high) vs. increase	decrease (high) vs. decrease
$1.5C_2$	decrease (high) vs. decrease	decrease (high) vs. decrease	decrease (high) vs. increase	decrease (low) vs. decrease
$1.5C_3$	increase (low) vs. decrease	increase (low) vs. decrease	decrease (high) vs. decrease	decrease (high) vs. decrease
High DB_3	increase (low) vs. decrease	increase (low) vs. decrease	increase (low) vs. increase	increase (low) vs. decrease
Only C_1*	decrease (high) vs. decrease	decrease (high) vs. decrease	decrease (high) vs. increase	decrease (high) vs. decrease
Only C_2*	decrease (high) vs. decrease	decrease (high) vs. decrease	decrease (high) vs. decrease	decrease (low) vs. decrease
Only C_3*	decrease+ (low) vs. increase	decrease+ (low) vs. increase	decrease (high) vs. decrease	decrease (high) vs. decrease

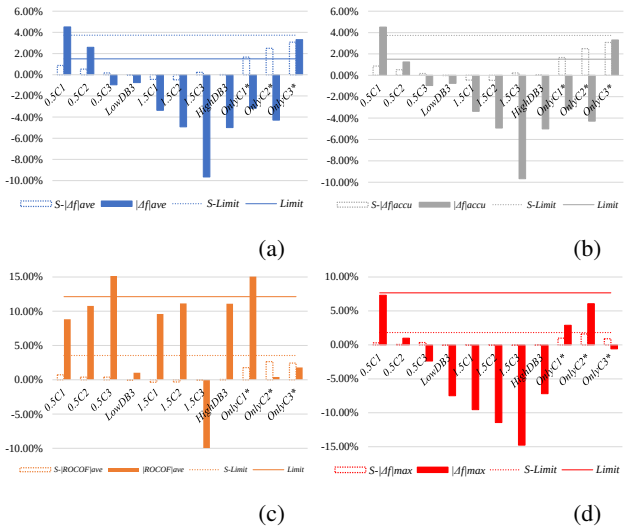

Fig. 5: Comparison of experimental and simulation results. All the results are referred to the base setup described in section III. The "S" denotes simulation results.

expected, this metric is strongly related to the effect of noise. Table II presents a comparison of the trends. Those marked with a positive sign (+) indicate that the simulation slightly mismatched the sensitivity results in Table I. The accuracy of the simulation is 90.91%. The global accuracy of the experimental tests, considering low-correlation comparisons, is 77.27%. Then, the accuracy of experimental tests, compared to simulation, is 85%. Additionally, if low correlation comparisons are neglected, the accuracy of experimental tests is also 85%. It is worth mentioning that high correlation mismatches are due to the frequency oscillations mentioned in Section III, since the mismatches occur mainly in $|ROCOF|_{ave}$.

IV. Conclusion

The frequency control from loads can contribute to face new challenges in current and future low-inertia power systems. The first contribution of the present work is a combined frequency control that enables railways to provide primary and supplementary frequency control, and virtual inertia. In the literature, loads were not considered to provide multiple types of control.

The second contribution of this work is the methodology used to assess these complex dynamics interactions of different controls of power systems. The approach is oriented toward analyzing the performance metrics using non-deterministic methods. Thus, the need to handle very detailed data is reduced. The simulation results confirm the benefits of the control and provide an insight of the overall behavior of controller interaction. It is noticeable that the operation range and selected metrics can considerably change the mutual influence among the controls. These results were used in experimental tests, performed with real commercial components. Although simulations and experiments do not share the same dynamics, the results show the same trend. This demonstrates the ability of the methodology to accurately assess the interaction in a grid with unknown dynamics, noise, and measurement errors, among other issues. Also, most of the control setups improve the frequency performance of the real grid. The small mismatches are due to the intrinsic oscillations of the GG, which can be equivalent to the implementation of the proposals in a real low-inertia and high-distorted grid. Both tests also provide insights into the influence of load events on the interactions. The C_1 parameter has the greatest influence in the simulation tests, but the parameter C_3 is highly relevant in the experimental tests. This is also explained by the frequency oscillations imposed by the GG. The experimental results validate the applicability and effectiveness of the proposed method under real conditions. It is worth mentioning that to assess certain types of interactions, some dynamics should not be oversimplified and the metrics should be properly designed.

Acknowledgments

Thanks to "Metro de Panamá" and the UTP for PML1 data.

Author Contributions

Author contributions according to Contributor Roles Taxonomy (CRediT): *Conceptualization:* J.A., F.W., S.M.; *Methodology:* J.A.; *Formal analysis:* J.A.; *Investigation:* J.A.; *Resources:* J.A., F.W.; *Data curation:* J.A.; *Writing - original draft:* J.A.; *Writing - review and editing:* J.A., F.W., S.W., V.H., S.M.; *Visualization:* J.A.; *Supervision:* F.W., S.W., S.M.; *Project administration:* S.W., S.M.; *Funding acquisition:* J.A., V.H., S.M.

References

[1] P. Denholm *et al.*, "The challenges of achieving a 100% renewable electricity system in the united states," *Joule*, vol. 5, pp. 1331–1352, 6 2021.

[2] J. Shair *et al.*, "Power system stability issues, classifications and research prospects in the context of high-penetration of renewables and power electronics," *Renewable and Sustainable Energy Reviews*, vol. 145, 7 2021.

[3] M. N. H. Shazon, Nahid-Al-Masood, and A. Jawad, "Frequency control challenges and potential countermeasures in future low-inertia power systems: A review," *Energy Reports*, vol. 8, pp. 6191–6219, 11 2022.

[4] N. Hatziargyriou *et al.*, "Definition and classification of power system stability - revisited & extended," *IEEE Transactions on Power Systems*, vol. 36, pp. 3271–3281, 7 2021.

[5] J. Fang *et al.*, "On the inertia of future more-electronics power systems," *IEEE Journal of Emerging and Selected Topics in Power Electronics*, vol. 7, pp. 2130–2146, 2019.

[6] M. Chen *et al.*, "Multitime-scale optimal dispatch of railway ftpss based on model predictive control," *IEEE Transactions on Transportation Electrification*, vol. 6, pp. 808–820, 2020.

[7] H. Yang *et al.*, "Distributed virtual inertia implementation of multiple electric springs based on model predictive control in dc microgrids," *IEEE Transactions on Industrial Electronics*, vol. 0046, 2021.

[8] Y. Yoo, Y. Al-Shawesh, and A. Tchagang, "Coordinated control strategy and validation of vehicle-to-grid for frequency control," *Energies*, vol. 14, 5 2021.

[9] M. Khan *et al.*, "Electric vehicles participation in load frequency control based on mixed h2/∞," *International Journal of Electrical Power and Energy Systems*, vol. 125, p. 106420, 2021.

[10] S. Yumiki *et al.*, "Autonomous vehicle-to-grid design for provision of frequency control ancillary service and distribution voltage regulation," *Sustainable Energy, Grids and Networks*, vol. 30, 6 2022.

[11] J. Araúz and S. Martinez, "Methodology for assessing the impact of regenerative braking energy injection of a direct current railway system on the distribution grid," *Electric Power Systems Research*, vol. 220, p. 109368, 7 2023.

[12] ——, "Contribution of the thermal inertia of trains to the primary frequency control of electric power systems," *Sustainable Energy, Grids and Networks*, vol. 34, p. 100988, 6 2023.

[13] ——, "Use of the thermal inertia of trains for contributing to primary frequency control and inertia of electric power systems," *IEEE Access*, vol. 11, pp. 57 099–57 116, 5 2023.

[14] ——, "Using the thermal inertia of trains for contributing to primary frequency control in grids with photovoltaic generation," in *2023 IEEE International Conference on Electrical Systems for Aircraft, Railway, Ship Propulsion and Road Vehicles & International Transportation Electrification Conference (ESARS-ITEC), Venice, Italy, 2023, pp. 1-6*. IEEE, 3 2023.

[15] ——, "Using the thermal inertia of trains for contributing to primary and supplementary frequency control in grids with high penetration of renewable generation," *IEEE Access*, vol. 12, pp. 63 271–63 281, 2024.

[16] P. Kundur, N. Balu, and M. Lauby, *Power System Stability and Control*, ser. EPRI power system engineering series. McGraw-Hill Education, 1994.

[17] IEEE Guide for Synchronous Generator Modeling Practices and Applications in Power System Stability Analyses. IEEE Std 1110-2002 (Revision of IEEE Std 1110-1991 [2003]): 1–72.

[18] M. Asad, S. Martinez, and J. A. Sanchez-Fernandez, "Diesel governor tuning for isolated hybrid power systems," *Electronics*, vol. 12, p. 2487, 2023.

[19] D. Ochoa and S. Martinez, "Contribución de los aerogeneradores de velocidad variable al control primario de frecuencia en sistemas de energía eléctrica," p. 164, 2019.

[20] "Recommended Practice for Excitation System Models for Power System Stability Studies," IEEE® Standard 421.5-1992, August, 1992.

[21] F. Kiessling, R. Puschmann, and A. Schmieder, *Contact Lines for Electric Railways: Planning, Design, Implementation*, 1st ed., B. Siemens Aktiengesellschaft and Munich, Eds. Publicis Corporate Publishing, Munich Erlangen, 2001.

[22] F. Du *et al.*, "Modeling and simulation of metro dc traction system with different motor driven trains," *Asia-Pacific Power and Energy Engineering Conference, APPEEC*, pp. 5–8, 2010.

[23] K. Almaksour *et al.*, "Comparison of dynamic models for a dc railway electrical network including an ac/dc bi-directional power station," *Mathematics and Computers in Simulation*, vol. 184, pp. 244–266, 2021.

[24] N. Mohan, T. M. Undeland, and W. P. Robbins, *Power Electronics: converters, application, and design*, 3rd ed. John Wiley & Sons, Inc, 1997.

[25] H. Alnuman, D. Gladwin, and M. Foster, "Electrical modelling of a dc railway system with multiple trains," *Energies*, vol. 11, 2018.

[26] R. N. Hofstädter *et al.*, "Heat capacity and heat transfer coefficient estimation for a dynamic thermal model of rail vehicles," *Mathematical and Computer Modelling of Dynamical Systems*, vol. 23, pp. 439–452, 2017.

[27] M. M. Eissa *et al.*, "Emergency frequency control by using heavy thermal conditioning loads in commercial buildings at smart grids," *Electric Power Systems Research*, vol. 173, pp. 202–213, 8 2019.

[28] H. Chen *et al.*, "Fractional-order pid load frequency control for power systems incorporating thermostatically controlled loads," in *Proceedings of 2021 IEEE 4th International Electrical and Energy Conference, CIEEC 2021*. Institute of Electrical and Electronics Engineers Inc., 5 2021.

[29] S. Subedi *et al.*, "Cost-benefit analysis of grid-supportive loads for fast frequency response," in *2023 IEEE PES Grid Edge Technologies Conference & Exposition (Grid Edge)*, 2023, pp. 1–5.

[30] Y. Son *et al.*, Hardware Implementation and Market Impacts of Grid-Supportive Functions in End-Use Loads. United States: N. p., 2023.

[31] C. Xiao *et al.*, "Transient power angle stability analysis and improvement strategy for parallel system of virtual synchronous generator and static var generator," *International Journal of Circuit Theory and Applications*, vol. September, no. n/a, pp. 1–17, 2023.

[32] C. Han *et al.*, "Grid synchronization control for grid-connected voltage source converters based on voltage dynamics of dc-link capacitor," *Journal of Modern Power Systems and Clean Energy*, pp. 1–12, 2023.

[33] L. Zeng, X. Shan, and Y. Wang, "A review of global sensitivity and its application in power systems," in *Second International Conference on Energy, Power, and Electrical Technology (ICEPET 2023)*, M. S. M. Saat and M. B. I. Reaz, Eds., vol. 12788, International Society for Optics and Photonics. SPIE, 2023, p. 127885P.

[34] A. Saltelli *et al.*, *Global Sensitivity Analysis. The Primer*, 1st ed. John Wiley & Sons, Ltd, 2007.

[35] F. Wiegel *et al.*, "Smart energy system control laboratory – a fully-automated and user-oriented research infrastructure for controlling and operating smart energy systems," *at - Automatisierungstechnik*, vol. 70, no. 12, pp. 1116–1133, 2022.

[36] R. Quint and D. Ramasubramanian, "Impacts of droop and deadband on generator performance and frequency control," *IEEE Power and Energy Society General Meeting*, vol. January, pp. 1–5, 2018.

[37] W. Daniel, *Applied Nonparametric Statistics*, 2nd ed., ser. Duxbury advanced series in statistics and decision sciences. PWS-KENT Pub., 1990. [Online]. Available: https://books.google.com.pa/books?id=0hPvAAAAMAAJ

BIOGRAPHIES

Jesús Araúz received the M.S. degree in electrical engineering, and the Ph.D. degree in electrical and electronics engineering from the UPM, Madrid, Spain, in 2021 and 2024, respectively. His research interests are railways and ancillary services in power systems.

Friedrich Wiegel leads the Smart Energy System Control Laboratory at the IAI at KIT while pursuing a Ph.D. in electrical engineering. His research interests include power system modeling, microgrid operation and automation, information and communication technology, and Power HIL.

Simon Waczowicz received the Ph.D. degree in mechanical engineering from KIT in 2018. Since then he heads the Research Platform Energy department at the IAI at KIT. His research interests include energy system design and operation, and time series analysis and forecasting.

Veit Hagenmeyer received the Ph.D. degree from Université Paris XI, Paris, France, in 2002. He is currently a Professor of Energy Informatics with the Faculty of Computer Science, and the Director of the IAI at KIT. His research interests include modeling, optimization and control of sector-integrated energy systems.

Sergio Martinez (M'02, SM'18) received the M.S. degree in industrial engineering and the Ph.D. degree in electrical engineering from the UPM in 1993 and 2001, respectively. He is a Professor with the Department of Electrical Engineering. His research interests include the provision of ancillary services from electrical equipment connected to power systems through power electronics.